



**HAL**  
open science

## Shigella-mediated oxygen depletion is essential for intestinal mucosa colonization

Jean-Yves Tinevez, Ellen T Arena, Mark Anderson, Giulia Nigro, Louise Injarabian, Antonin André, Mariana Ferrari, François-Xavier Campbell-Valois, Anne Devin, Spencer Shorte, et al.

### ► To cite this version:

Jean-Yves Tinevez, Ellen T Arena, Mark Anderson, Giulia Nigro, Louise Injarabian, et al.. Shigella-mediated oxygen depletion is essential for intestinal mucosa colonization. *Nature Microbiology*, 2019, 4 (11), pp.2001-2009. 10.1038/s41564-019-0525-3. hal-02402067

**HAL Id: hal-02402067**

**<https://hal.science/hal-02402067>**

Submitted on 11 Jun 2020

**HAL** is a multi-disciplinary open access archive for the deposit and dissemination of scientific research documents, whether they are published or not. The documents may come from teaching and research institutions in France or abroad, or from public or private research centers.

L'archive ouverte pluridisciplinaire **HAL**, est destinée au dépôt et à la diffusion de documents scientifiques de niveau recherche, publiés ou non, émanant des établissements d'enseignement et de recherche français ou étrangers, des laboratoires publics ou privés.



Distributed under a Creative Commons Attribution - NonCommercial 4.0 International License



1 **Title: *Shigella*-mediated oxygen depletion is essential for intestinal**  
2 **mucosa colonization**

3

4 **Authors**

5 Jean-Yves Tinevez<sup>1,2,†</sup>, Ellen T Arena<sup>3,4,€,†</sup>, Mark Anderson<sup>3,4</sup>, Giulia Nigro<sup>3,4</sup>, Louise  
6 Injarabian<sup>3,5</sup>, Antonin André<sup>3,5</sup>, Mariana Ferrari<sup>3,4</sup>, François-Xavier Campbell-Valois<sup>3,4,£</sup>, Anne  
7 Devin<sup>5</sup>, Spencer L Shorte<sup>1,6</sup>, Philippe J Sansonetti<sup>3,4,7</sup>, Benoit S Marteyn<sup>3,4,5\*</sup>

8

9 **Affiliations**

10 <sup>1</sup>UTechS PBI (Imagopole), C2RT, Institut Pasteur, Paris, France

11 <sup>2</sup>Image Analysis Hub, C2RT, Institut Pasteur, Paris, France

12 <sup>3</sup>Unité de Pathogénie Microbienne Moléculaire, Institut Pasteur, Paris, France

13 <sup>4</sup>INSERM Unité 1202, Paris, France

14 <sup>5</sup>Université Bordeaux, IBGC, CNRS UMR 5095, Bordeaux, France

15 <sup>6</sup>Institut Pasteur Korea, Scientific Direction, 16, Daewangpangyo-ro 712 beon-gil

16 Bundang-gu, Seongnam-si, Gyeonggi-do, 13488 Rep. of Korea

17 <sup>7</sup>Collège de France, Paris, France

18 <sup>€</sup>Current affiliation: Laboratory for Optical and Computational Instrumentation (LOCI),  
19 University of Wisconsin - Madison, 1675 Observatory Drive, Madison, WI 53706, USA

20 <sup>£</sup>Current affiliation: University of Ottawa, Faculty of Science, Department of Chemistry and  
21 Biomolecular Sciences and Faculty of Medicine, Department of Biochemistry, Microbiology  
22 and Immunology, Ottawa, Ontario, Canada

23 †These authors contributed equally to this work.

24

25 \* Corresponding author: Benoit Marteyn (marteyn@pasteur.fr), Institut Pasteur, Unité PMM,  
26 Paris, France; Phone +33 1 45488308; Fax +33 1 45488953.

27

28 **Abstract.**

29

30 **Pathogenic enterobacteria face various oxygen (O<sub>2</sub>) levels during intestinal**  
31 **colonization from the O<sub>2</sub>-deprived lumen to oxygenated tissues. Using *Shigella***  
32 ***flexneri* as a model, we had previously demonstrated that epithelium invasion**  
33 **is promoted by O<sub>2</sub> in a Type III secretion system (T3SS)-dependent manner<sup>1</sup>.**  
34 **However, subsequent pathogen adaptation to tissue oxygenation modulation**  
35 **remained unknown. Assessing single-cell distribution, together with tissue**  
36 **oxygenation, we demonstrate here that the colonic mucosa O<sub>2</sub> is actively**  
37 **depleted by *Shigella flexneri* aerobic respiration, not host neutrophils, during**  
38 **infection, leading to the formation of hypoxic foci of infection. This process is**  
39 **promoted by T3SS inactivation in infected tissues, favoring colonizers over**  
40 **explorers. We identify the molecular mechanisms supporting infectious**  
41 **hypoxia induction, and we demonstrate here how enteropathogens optimize**  
42 **their colonization capacity in relation to their ability to manipulate tissue**  
43 **oxygenation during infection.**

44 Pathogenic enterobacteria virulence and first-line immune cells', particularly  
45 neutrophils', survival and function are highly modulated by oxygen (O<sub>2</sub>)<sup>1,2,3,4</sup>. Most  
46 virulent enterobacteria (*Shigella* spp., *Listeria* spp., *Salmonella* spp., pathogenic  
47 *E. coli*, or *Yersinia pestis*) are well adapted to these changing microenvironments<sup>5</sup>,  
48 suggesting adaptability to various O<sub>2</sub> levels represents a selective advantage crucial  
49 for their infectious capacity. The colonization process involves three key steps:  
50 degradation of the mucus layer, invasion of the epithelium mediated by the T3SS,  
51 and formation of primary foci of infection. We previously demonstrated that *S. flexneri*  
52 T3SS activation requires O<sub>2</sub>, which diffuses on the epithelium surface<sup>1</sup>. However,  
53 tissue oxygenation modulation during the dissemination of enteropathogens and its  
54 impact on colonization or immune response efficiency remains largely unknown,  
55 although hypoxia has been previously reported in a TNBS colitis model of  
56 inflammation<sup>6</sup>.

57 In this work, we show that oxygen is depleted during tissue colonization by  
58 enteropathogens, using *S. flexneri* as a model, leading to the formation of hypoxic  
59 foci of infection. We designed a quantitative image analysis method allowing the  
60 assessment of tissue oxygenation at a single-cell level for both bacteria and  
61 neutrophils. We demonstrate that *S. flexneri* aerobic respiration is essential for O<sub>2</sub>  
62 depletion within the colonic mucosa, not neutrophils, as previously demonstrated in a  
63 non-infectious model of inflammation<sup>7</sup>. We show that formation of hypoxic foci of  
64 infection is the primary *S. flexneri* colonization strategy, which is promoted by the  
65 repression of T3SS activity. Our results demonstrate that the interaction between  
66 *S. flexneri* and immune cells occurs mainly in the absence of O<sub>2</sub>. We anticipate our  
67 results will have a significant impact on new vaccine and antibiotic development  
68 strategies, as well as reappraisal of immune response and host-pathogen  
69 interactions in low O<sub>2</sub> conditions.

70

71 We recently observed that hypoxia was induced within the colonic mucosa  
72 upon *S. flexneri* infection<sup>8</sup> using a hypoxia reporter, EF5<sup>9</sup>. Here, measuring relative  
73 hypoxia levels from the epithelial surface to the submucosa (Supplementary Table 1),  
74 we confirmed this preliminary observation (Figure 1a) and demonstrated that during  
75 infection, compared to basal conditions, the degree of hypoxia increased significantly  
76 to a depth of 130 μm (Figure 1b, *p* < 0.05). In basal conditions, the 'physiological

77 hypoxic status' of the epithelium was confirmed, as previously reported in the  
78 mouse<sup>6,7</sup> (Figure 1b, uninfected tissues).

79 Taking into account the potential heterogeneity of the bacteria population<sup>10</sup>,  
80 we developed a quantitative imaging strategy at a single-bacteria level, as previously  
81 reported<sup>11</sup>, to localize individual bacteria and assess hypoxia levels (Figure 1c and  
82 Supplementary Figure 1a-c). First, we revealed that most bacteria (99.71%,  
83 Supplementary Figure 1a) were located within foci of infection formed in the colonic  
84 extracellular matrix ('clustered' bacteria, defined as having at least 6 neighboring  
85 bacteria within 16  $\mu\text{m}$ ) not dispersed within the mucosa ('dispersed' bacteria, defined  
86 as having a closest neighboring bacteria beyond 30  $\mu\text{m}$ , Figure 1c and  
87 Supplementary Figure 1a). We demonstrated that *S. flexneri* faced hypoxic  
88 conditions specifically within foci of infection, not when dispersed elsewhere in the  
89 mucosa (Figure 1d-f,  $p < 10^{-10}$ ). This result implies that *S. flexneri* adaptation to low-  
90  $\text{O}_2$  levels is crucial for tissue colonization. We demonstrated that a *S. flexneri*  $\Delta fnr$   
91 mutant strain (FNR, which mediates the adaptation of *S. flexneri* to anaerobiosis<sup>1</sup>) did  
92 not propagate within foci of infection and was avirulent (Supplementary Figure 2a),  
93 as previously demonstrated<sup>1</sup>; also, the neutrophil population was reduced, a sign of  
94 limited inflammation (Supplementary Figure 2a). In a rabbit ileal loop model, we  
95 confirmed that FNR was specifically required for *S. flexneri* propagation in an  
96 inflammatory environment, but not mandatory for its fitness within the intestinal lumen  
97 (Supplementary Figure 2b).

98 Neutrophils represent the most abundant immune cell population recruited  
99 upon *Shigella* infection, and their activation has been previously identified as  
100 responsible for hypoxia induction in a TNBS colitis model of inflammation<sup>7</sup>.  
101 Neutrophils were specifically labeled with MUB<sub>40</sub>, (or Myelotracker, a neutrophil  
102 lactoferrin marker<sup>12</sup>), allowing single-cell analyses (Figure 1g). We observed that  
103 neutrophils were in closest proximity to 'clustered' bacteria compared to 'dispersed'  
104 bacteria (Figure 1h) and that the level of hypoxia quantified at a single-neutrophil  
105 level was significantly higher when located in the vicinity of 'clustered' bacteria  
106 (Figure 1i). Hypoxia levels measured at a single-bacteria level around 'clustered' and  
107 'dispersed' *S. flexneri* remained similar in conventional and neutropenic animals  
108 (Figure 2a-b), suggesting that neutrophil contribution is not an essential factor for  
109 hypoxia induction. As expected, a significantly reduced amount of neutrophils were

110 detected in the infected colonic mucosa of neutropenic animals; the *S. flexneri*  
111 population was only mildly reduced (Supplementary Figure 2c). Neutrophil hypoxia  
112 levels were compared to the closest bacteria hypoxia profiles; for more than 95% of  
113 neutrophils, hypoxia levels were not found to be significantly higher than the hypoxia  
114 generated by bacteria in their vicinity (Supplementary Figure 2d).

115

116 Since neutrophils' contribution seemed limited, O<sub>2</sub> consumption mediated by  
117 *S. flexneri* was investigated as a potential cause of local O<sub>2</sub> depletion observed within  
118 foci of infection. *S. flexneri* population density in foci was estimated from confocal  
119 images to be  $3.9 \cdot 10^9 \pm 2.7 \cdot 10^9$  cell/mL for 'clustered' bacteria, compared to  
120  $1.3 \cdot 10^6 \pm 1.1 \cdot 10^6$  cell/mL for bacteria 'dispersed' in the tissue (Figure 2c-d). The  
121 impact of bacterial density on *S. flexneri* O<sub>2</sub> consumption kinetics was then assessed  
122 *in vitro* using a dedicated device allowing the inoculation of bacteria in a sealed  
123 anoxic tube containing culture medium stabilized at 40 mmHg O<sub>2</sub>, reflecting  
124 estimated physiological O<sub>2</sub> levels<sup>13</sup> (Figure 2e). O<sub>2</sub> consumption rate was correlated  
125 to the *S. flexneri* population cell density (Figure 2f). At a cell density measured within  
126 foci of infection (between  $1 \cdot 10^9$  and  $5 \cdot 10^9$  cell/mL), complete O<sub>2</sub> depletion by  
127 *S. flexneri* occurred rapidly ( $t_{\text{anoxia}} = 2.3 \pm 1.1$  min, Figure 2f); similar results were  
128 obtained with other pathogenic enterobacteria, including *E. coli*, *S. typhimurium*,  
129 *L. monocytogenes*, and *Y. pestis*, though not with *Lactobacillus casei*, an  
130 aerotolerant anaerobe (Supplementary Figure 3). When a similar experiment was  
131 conducted at a density corresponding to the 'dispersed' population, complete O<sub>2</sub>  
132 depletion was not achieved over the measurement period (Figure 2f). The co-  
133 incubation of neutrophils with *S. flexneri* at a pathophysiological cell density  
134 ( $8.1 \cdot 10^7 \pm 5.4 \cdot 10^7$  cell/mL, Figure 2d) had no impact on the timing of complete O<sub>2</sub>  
135 depletion compared to *S. flexneri* alone (clustered,  $t_{\text{anoxia}} = 2.4 \pm 1.0$  min,  $p > 0.05$ ,  
136 Figure 2g). A mild increase of O<sub>2</sub> consumption was observed when co-incubating  
137 neutrophils with *S. flexneri* at a cell density corresponding to the 'dispersed'  
138 population or heat-killed bacteria ( $t = 10$  min,  $p < 0.01$  and  $p < 0.05$ , respectively),  
139 although complete O<sub>2</sub> depletion was not achieved over the measurement period  
140 (Figure 2g). We demonstrate here that O<sub>2</sub> depletion during infection seems driven by  
141 *S. flexneri*, while neutrophils contribute comparatively much less.

142

143 We reasoned that *S. flexneri* aerobic respiration is responsible for the O<sub>2</sub>  
144 depletion observed *in vivo*. At the end of the aerobic respiratory chain, O<sub>2</sub> is reduced  
145 to H<sub>2</sub>O by terminal cytochrome oxidases<sup>14</sup>: *S. flexneri* expresses two cytochrome  
146 oxidases named *bd-I* (CydAB) and *bd-II* (AppCB), similarly to *E. coli*, (*S. flexneri*  
147 *cyoAB* genes are truncated) (Figure 3a). Therefore, we engineered *S. flexneri*  
148  $\Delta$ *cydAB* and  $\Delta$ *appCB* mutants and noted that their cellular morphologies were  
149 indiscernible from the wild-type (Supplementary Figure 4a).

150

151 We showed that the *bd-I* complex (CydAB), but not the *bd-II* complex  
152 (AppCB), was essential for *S. flexneri*'s ability to consume O<sub>2</sub> (Figure 3b).  
153 Consistently, cytochromes *b* and *d* expressed by *S. flexneri* belong mainly to the *bd-I*  
154 complex (Supplementary Figure 4b), and *S. flexneri*  $\Delta$ *cydAB* displayed a growth  
155 defect in the presence of O<sub>2</sub> compared to the wild-type strain, confirming that aerobic  
156 respiration is defective in this mutant (Supplementary Figure 4c). The *S. flexneri*  
157  $\Delta$ *cydAB* (*bd-I*) mutant was not virulent *in vivo*, O<sub>2</sub> depletion was not observed, and  
158 foci of infection were not formed in the colonic mucosa (Figure 3c-d); although it  
159 remained invasive and was phagocytized by neutrophils as per the wild-type strain *in*  
160 *vitro* (Supplementary Figure 4d). Consistent with previous results (Figure 2f-g), the  
161 co-incubation of neutrophils (with or without DPI, a neutrophil NADPH oxidase  
162 inhibitor) with *S. flexneri*  $\Delta$ *appCB* (*bd-II*) had no impact on timing of anoxia induction  
163 (Supplementary Figure 4e). When similar experiments were conducted with *S.*  
164 *flexneri*  $\Delta$ *cydAB* or upon activation with N-Formyl-Met-Leu-Phe (FmlF), a mild  
165 increase of oxygen consumption was observed and abolished by DPI  
166 (Supplementary Figure 4e,  $p < 0.05$ ); although anoxia was not reached in both  
167 conditions over the measurement period.

168 We confirmed that GLUT-1, a hypoxia-induced glucose transporter<sup>7</sup>, was  
169 overexpressed in non-infected epithelial cells (physiological hypoxia), but also within  
170 *S. flexneri* foci of infection (Figure 3f and Supplementary Figure 5a) though not upon  
171 *S. flexneri*  $\Delta$ *cydAB* mutant infection (Supplementary Figure 5a). To confirm that  
172 *S. flexneri*  $\Delta$ *cydAB* avirulence was caused by its defect in O<sub>2</sub> consumption, we co-  
173 infected guinea pigs with *S. flexneri* pGFP wild-type and  $\Delta$ *cydAB* pDsRed mutant  
174 strains. We confirmed that hypoxia was induced within foci of infection (GLUT-1  
175 stabilization, Figure 3f), mediated by *S. flexneri* wild-type strain, and we

176 demonstrated that, in this context, the *S. flexneri*  $\Delta$ *cydAB* mutant was able to  
177 colonize the colonic mucosa together with the wild-type strain (Figure 3f and  
178 Supplementary Figure 5b). The relative amount of *S. flexneri* wild-type and  $\Delta$ *cydAB*  
179 mutant strains in the lumen (comparing plasmid-cured BS176 and BS176 $\Delta$ *cydAB*  
180 mutant strains, Figure 3f and Supplementary Figure 5b) or within the colonic mucosa  
181 (comparing M90T and M90T $\Delta$ *cydAB* mutant strains, Figure 3f and Supplementary  
182 Figure 5b) was similar (Competitive Index value around 1), as observed *in vitro* under  
183 anoxic conditions (Figure 3g). We therefore confirmed our hypothesis that *S. flexneri*  
184 aerobic respiration was the primary cause of hypoxia induction *in vivo*, explaining its  
185 essential role for tissue colonization<sup>15</sup>. The ability of *S. flexneri* to grow in the  
186 absence of O<sub>2</sub> supports the expansion of foci, whose formation appears to be the  
187 preferential strategy for tissue colonization (composed of 99.71% total bacteria,  
188 Supplementary Figure 1a).

189

190 We hypothesized that the repression of *S. flexneri*'s dissemination capacity  
191 may promote foci of infection extension by favoring colonizing over exploring  
192 bacteria. *S. flexneri*'s ability to invade host cells relies on the T3SS, whose activity is  
193 significantly reduced in hypoxic conditions<sup>1</sup>. To assess the level of T3SS activity of  
194 individual bacterium within colonic tissues, we measured the fluorescence signal  
195 produced by a *S. flexneri* strain harboring the pTSAR plasmid, which has a fast-  
196 maturing eGFP under the control of a T3SS activity-dependent promoter<sup>16</sup>.

197

198 The positive correlation between O<sub>2</sub> availability and the T3SS-activity in the  
199 presence of the secretion inducer Congo red (congo red, +CR) was confirmed *in vitro*  
200 (fast-maturing eGFP fluorescent signal and IpaB secretion, Figure 4a-b,  $p < 0.001$ ).  
201 We also previously confirmed oxygen-dependent type III secretion of effectors *in vitro*  
202 by western blot<sup>1</sup>. The activity of *S. flexneri* T3SS was also assessed *in vivo* within  
203 foci of infection (Figure 4c). Performing a single-bacteria analysis, we demonstrated  
204 that *S. flexneri* T3SS was mostly inactive in infected tissues (87.55% total bacteria,  
205 Figure 4d-e,  $n = 265$  bacteria). These results confirm that hypoxic conditions  
206 encountered in foci of infection blocks T3SS activation, hence limiting *S. flexneri*  
207 dissemination to adjacent host cells and promoting tissue colonization through foci  
208 expansion.

209

210 Here we show that intestinal mucosa colonization by *S. flexneri* occurs through  
211 the formation and expansion of hypoxic foci of infection. In summary, while O<sub>2</sub> is  
212 essential for *S. flexneri* T3SS-dependent epithelium invasion<sup>1</sup>, its depletion is  
213 conversely mandatory for subsequent tissue colonization. The ability of *S. flexneri* to  
214 survive this low-oxygenated environment, as well as the associated blockade of the  
215 T3SS, contributes to the expansion of foci of infection.

216 Our results reveal that the adaptation of invasive pathogens to various O<sub>2</sub>  
217 levels is essential for tissue colonization. In fact, to our knowledge, pathogenic  
218 microorganisms that are not facultative anaerobes are not invasive. We demonstrate  
219 that O<sub>2</sub> depletion by pathogenic enterobacteria may be considered a community  
220 behavior<sup>17</sup>, querying previous concepts such as the O<sub>2</sub> availability in colonic  
221 inflammation models and bacteria adaptation to these pathophysiological  
222 environments<sup>18</sup>. In particular, improved methods will be required to study the  
223 population heterogeneity within foci in regards to O<sub>2</sub> levels. For example, more than  
224 40% of individual bacteria were neither ‘clustered’ nor ‘dispersed’ in neutropenic  
225 animals (Supplementary Table 1), highlighting the importance of foci formation in  
226 response to neutrophil recruitment and antimicrobial activity.

227 O<sub>2</sub> depletion by pathogenic enterobacteria is expected to modulate the  
228 survival and function of immune cells<sup>19,20</sup>, particularly neutrophils<sup>2,3,4</sup>; important O<sub>2</sub>-  
229 dependent antimicrobial functions, such as ROS production, are likely to be altered.  
230 The contribution of alternative electron transfer machineries for oxygen-depletion and  
231 enteropathogen virulence, such as the recently described *Listeria monocytogenes*  
232 extracellular electron transport (EET)<sup>21</sup>, requires further investigation. The respective  
233 contributions of enteropathogens, commensal flora, and host cells (*i.e.* neutrophil  
234 activation, epithelial cell death, etc.) in oxygen depletion may be further investigated  
235 in other acute or chronic models of inflammation. In conclusion, this “battle to  
236 breathe” is anticipated to be crucial for the outcome of infection and will have to be  
237 taken into account in the development of truly effective antibiotics or vaccines  
238 targeting pathogens in low-O<sub>2</sub> environments for efficient clearance or protection.

239

240 **Acknowledgements.**



241 We acknowledge France-BioImaging infrastructure supported by the French National  
242 Research Agency (ANR-10-INBS-04, Imagopole, JYT), ANR JCJC 2017-17-CE15-  
243 0012 (BSM), and the European Research Council (ERC Grant: 2009-AdG  
244 HOMEOPATH, PJS). E.T.A. was a Pasteur Foundation and Pasteur-Roux Fellow.

245

246 **Competing interest statement**

247 The authors declare no competing interests

248

249 **Author contributions**

250 BSM, JYT and ETA designed the experiments, interpreted the data, and wrote the  
251 paper. MA designed *Shigella* mutants. GN, LI, AA, MF and FXCV contributed to their  
252 study *in vitro* and *in vivo*. JYT conducted quantitative analysis of the data. AD, SLS  
253 and PSJ contributed to data interpretation.

254

255 **Figure legends.**

256 **Figure 1. Hypoxia is specifically induced by *Shigella* within foci of infection.**

257 **a.** Hypoxia was detected in guinea pig colonic mucosa infected with *S. flexneri* 5a  
258 pGFP strain (green) using the EF5 reporter<sup>9</sup>. EF5 was immunodetected with an a-  
259 EF5-Cy3 (red); neutrophils were labeled with the Myelotracker-Dylight405<sup>12</sup> marker  
260 (or Myelotracker-Alexa405<sup>12</sup>, blue). Scale bar: 50  $\mu$ m.

261 **b.** Hypoxia profiles through the colonic mucosa were reported. The EF5 level is  
262 reported as mean over all aligned profiles (thick lines)  $\pm$  standard deviation (shaded  
263 area) against tissue depth ( $n = 128, 61$  and  $48$  profiles averaged for respectively the  
264 M90T, uninfected and no-EF5 conditions). The gray segments atop the curves  
265 represent the range of depths for which the EF5 levels are significantly different  
266 between the M90T and uninfected conditions (two-sided Student t-test,  $p < 0.05$ ).

267 **c.** Individual bacteria were detected by quantitative image analysis (red dot, see  
268 Supplementary Figure 1a), and two populations of *S. flexneri* were defined: as  
269 'dispersed' if its closest neighbor was located beyond 30  $\mu$ m or as 'clustered' if at  
270 least 6 bacteria were within a 16  $\mu$ m diameter, forming a focus of infection. Scale bar:  
271 20  $\mu$ m.

272 **d.** Detection of 'clustered' and 'dispersed' bacteria populations within the colonic  
273 mucosa. Scale bar: 50  $\mu$ m.

274 **e-f.** Hypoxia levels were compared at single 'dispersed' and 'clustered' bacteria  
275 levels by quantitative image analysis. Scale bar: 20  $\mu$ m. Hypoxia levels were  
276 significantly higher around 'clustered' compared to 'dispersed' bacteria (ANOVA 1-  
277 way test + Tukey test, on  $n = 61119, 186$  and  $11400$  bacteria, respectively for the  
278 clustered+EF5, dispersed+EF5 and no-EF5 conditions, see Supplementary Table 2).  
279 The no-EF5 signal was measured on infected tissues not stained with EF5.

280 **g.** Individual neutrophils (orange dot), stained with Myelotracker-Dylight405<sup>12</sup>, were  
281 localized in tissue by quantitative image analysis.

282 **h.** Neutrophils were found closer to 'clustered' bacteria compared to 'dispersed'  
283 bacteria (distance from  $n = 61119$  and  $186$  bacteria to the closest neutrophil for  
284 respectively the 'clustered' and 'dispersed' bacteria,  $p < 10^{-10}$ ).

285 **i.** The hypoxia level detected around neutrophils (averaged over the 5 closest) was  
286 higher around 'clustered' bacteria compared to 'dispersed' bacteria (EF5 levels

287 around the 5 closest neutrophils, measured for  $n = 61119$ , 186 and 11400 bacteria,  
288 respectively for the clustered+EF5, dispersed+EF5 and no-EF5 conditions,  $p \sim 10^{-10}$ .  
289 \*\*\* indicates  $p < 0.001$ . In the box-plots of panels f and h, the central mark indicates  
290 the median, and the bottom and top edges of the box indicate the 25th and 75th  
291 percentiles, respectively. The whiskers extend to the most extreme data points not  
292 considered outliers, and the outliers are not plotted. Outliers are data points that are  
293 further away than 1.5 times the range from the 1st to the 3rd quartile, respectively  
294 above or below the 3rd and 1st quartile.

295

296 **Figure 2. Neutrophils are not essential for O<sub>2</sub> depletion in infected tissues,**  
297 **which is mainly caused by *Shigella* aerobic respiration.**

298 **a.** *S. flexneri* pGFP (green) foci of infection were detected in conventional (8 animals,  
299 28 acquisitions) and neutropenic (3 animals, 7 acquisitions) guinea pig colonic  
300 mucosa. Neutrophils were labeled with Myelotracker-Dylight405<sup>12</sup> (blue) and hypoxia  
301 with an  $\alpha$ -EF5-Cy3 (red). Scale bar: 50  $\mu$ m.

302 **b.** Hypoxia levels around 'clustered' bacteria were comparable between conventional  
303 vs neutropenic animals ( $p < 0.0001$ , see Supplementary Table 3).

304 **c-d.** Cell density of 'clustered' (in foci of infection) and 'dispersed' *S. flexneri* pGFP  
305 (green) populations were calculated *in vivo* (expressed as mean  $\pm$  S.D). Neutrophils  
306 were labeled with Myelotracker-Dylight405<sup>12</sup> (blue) and hypoxic areas with an  $\alpha$ -EF5-  
307 Cy3 (red). Scale bar: 2  $\mu$ m. For clustered bacteria, the density is calculated as the  
308 number of bacteria around each clustered bacterium within 16  $\mu$ m for 61119 bacteria.  
309 For dispersed bacteria and neutrophils, the density is calculated as the number of  
310 dispersed bacteria ( $n = 37$  loci imaged), respectively neutrophils ( $n = 16$  loci imaged),  
311 divided by the imaged tissue volume.

312 **e.** O<sub>2</sub> consumption rates were assessed *in vitro* with an oximeter in a RPMI 1640 +  
313 10 mM HEPES culture medium stabilized at 40 mmHg (hypoxic chamber) in tubes  
314 sealed under anoxic conditions (see Methods). Exponentially grown bacterial cultures  
315 were inoculated at the indicated concentration ( $t = 0$ ).

316 **f.** O<sub>2</sub> depletion rate was correlated with *S. flexneri* bacterial density. O<sub>2</sub> tensions  
317 (expressed as mean  $\pm$  S.D.) were assessed at indicated cell densities surrounding  
318 'clustered' and 'dispersed' population densities calculated *in vivo* (see **d.**) or in the  
319 presence of  $5 \cdot 10^9$  heat-killed *S. flexneri* ( $n = 3$  independent experiments).

320 **g.** O<sub>2</sub> depletion rate (O<sub>2</sub> tensions expressed as mean ± S.D., *n* = 3 independent  
321 experiments) in the presence of *S. flexneri* and neutrophils (PMNs,  
322 8.10<sup>7</sup> neutrophils/mL). In the presence of 1.10<sup>6</sup> *S. flexneri*/mL or 5.10<sup>9</sup> heat-killed *S.*  
323 *flexneri*/mL, anoxia was not reached over the measurement period, although  
324 neutrophil O<sub>2</sub>-consumption was observed (10 min, see Supplementary Table 4).  
325

326 **Figure 3. Aerobic respiration is required for hypoxia induction and efficient**  
327 **colonic mucosa colonization by *Shigella in vivo*.**

328 **a.** Genetic organization of cytochrome oxidases (*bo<sub>3</sub>*, *bd-I* and *bd-II*) encoding genes  
329 in *Escherichia coli* K12 and *Shigella flexneri* 5a. *cyoA* and *cyoB* genes are not  
330 functional in *S. flexneri* due to genetic insertions.

331 **b.** *S. flexneri* 5a Δ*cydAB* (*bd-I*) was unable to consume O<sub>2</sub> *in vitro* in a RPMI 1640 +  
332 10 mM Hepes medium stabilized at a pO<sub>2</sub> = 40 mmHg and had a growth defect in  
333 the presence of O<sub>2</sub> (*n* = 3 independent experiments, *p* < 10<sup>-8</sup>, 2-way ANOVA test, see  
334 Supplementary Figure 4c and Supplementary Table 5). O<sub>2</sub> tensions expressed as  
335 mean ± S.D.

336 **c.** *S. flexneri* 5a Δ*cydAB* (*bd-I*) pGFP (green) was avirulent *in vivo* compared to wild-  
337 type and Δ*appCB* (*bd-II*) mutant strains. Hypoxia was detected with a-EF5-Cy3 (red),  
338 neutrophils with Myelotracker-Dylight405<sup>12</sup> (blue). Scale bar: 50 μm. This experiment  
339 was repeated independently three times with similar results.

340 **d.** Tissues infected with the Δ*cydAB* strain were not inflamed as compared to the  
341 wild-type strain, as indicated by the presence of solid stools in the colon lumen  
342 (mean ± S.D., *p* > 0.8, see Supplementary Table 6).

343 **e.** The number of foci of infection was significantly reduced in tissues infected by the  
344 Δ*cydAB* strain compared to the wild-type strain (mean ± S.D., *p* < 10<sup>-4</sup>, see  
345 Supplementary Table 7).

346 **f.** GLUT-1 was detected with a monoclonal antibody (magenta) within *S. flexneri* 5a  
347 pGFP (green) hypoxic foci of infection. *S. flexneri* 5a Δ*cydAB* pDsRed (red) was able  
348 to colonize the colonic mucosa upon co-infection with the wild-type strain (*S. flexneri*  
349 5a pGFP). Plasmid-cured BS176 and BS176Δ*cydAB* remain in the luminal  
350 compartment. Neutrophils were labeled with Myelotracker-Dylight405<sup>12</sup> (blue). Scale  
351 bar: 70 μm. See Supplementary Figure 5 for extended imaging. This experiment was  
352 repeated independently three times with similar results.

353 **g.** M90T/M90T $\Delta$ *cydAB* and BS176/BS176 $\Delta$ *cydAB* Competitive Indexes were  
354 determined in co-cultures *in vitro* (-O<sub>2</sub> conditions) and upon guinea pig co-infection *in*  
355 *vivo* (lumen and colonic mucosa). CI=1 means no growth difference (mean  $\pm$  S.D.,  
356 n=5 biologically independent animal samples). \*\*\* indicates  $p < 0.001$ .

357

358 **Figure 4. *S. flexneri* T3SS is inactive in the colonic mucosa, supporting foci of**  
359 **infection extension.**

360 **a-b.** O<sub>2</sub>-dependent modulation of *S. flexneri* Type III secretion system (T3SS)<sup>1</sup> was  
361 confirmed *in vitro* in the presence of congo red (0.01%) using the activity reporter  
362 pTSAR<sup>16</sup> (bacteria are constitutively cyan (CFP); bacteria with an active T3SS have a  
363 high pTSAR signal (eGFP, green, #), not bacteria with an inactive T3SS (\*)); T3SS  
364 was active at a GFP signal intensity above 900 AU, as indicated by a 1-way ANOVA  
365 test (see Supplementary Table 8, \*\*\* indicates  $p < 0.001$ . Red lines and black bars:  
366 mean  $\pm$  standard deviation.)

367 **c.** T3SS activity was assessed at a single-bacteria level *in vivo*, in hypoxic foci of  
368 infection formed by *S. flexneri* pTSAR This experiment was repeated independently  
369 three times with similar results.

370 **d-e.** Bacteria with an active T3SS are indicated in the green channel (#) in Z-stack  
371 image series, and bacteria with an inactive T3SS are indicated in the cyan channel  
372 (\*). Most of *S. flexneri* pTSAR individual bacteria detected within hypoxic foci of  
373 infection have an inactive T3SS (\*, 87.66% total population with eGFP signal  
374 intensity above 900 AU,  $n = 286$  bacteria. Red and black bars are mean  $\pm$  S.D.  $n = 3$   
375 biologically independent animal samples).

376

## 377 **Material and Methods.**

### 378 **Bacterial strains, growth conditions.**

379 *Shigella flexneri* 5a (*Shigella*) strains (wild-type M90T, plasmid-cured BS176 M90T $\Delta$ *fnr* mutant, and  
380 BS176 $\Delta$ *fnr* mutant) and *Staphylococcus aureus* were propagated in Trypticase soy media (TCS,  
381 Oxoid) or on TCS plates, supplemented with Congo Red (0.01%, Sigma) for *Shigella* strains.  
382 *Escherichia coli*, *Salmonella typhimurium*, and *Listeria monocytogenes* were cultured in Luria Bertani  
383 (LB) medium. *Lactobacillus casei* was grown in deMan, Rogosa and Sharpe (MRS) broth (Sigma-  
384 Aldrich). *S. flexneri* M90T was used as a wild-type *Shigella* strain. Targeted deletion of *appCB* and  
385 *cydAB* genes was performed using  $\lambda$  red recombination using the following primers *appCB*1  
386 (5'-ATGTGGGATGTCATTGATTTATCGCGCTGGCAGTTTGCTCCATATGAATATCCTCCTTAGTTCC  
387 -3') and *appCB*2  
388 (5'-TTAGTACAACCTCGTTTTTGTACGGCGGAGAGTTTCTGTTGTGTAGGCTGGAGCTGCTTC-3')  
389 with plasmid pKD3 to generate a PCR product containing a chloramphenicol resistance cassette  
390 flanked on each end with 50bp corresponding to the *S. flexneri appCB* genes. Primers *cydAB*1  
391 (5'-TTAGTACAGAGAGTGGGTGTTACGTTCAATATCTTCTTTGCATATGAATATCCTCCTTAGTTCC-  
392 3') and *cydAB*2  
393 (5'-ATGTTAGATATAGTCGAACTGTCGCGCTTACAGTTTGCCTGTGTAGGCTGGAGCTGCTTC-3')  
394 were used with plasmid pKD4 to generate a PCR product containing a kanamycin resistance cassette  
395 flanked on each end with 50bp corresponding to the *S. flexneri cydAB* genes. KO generation was  
396 performed under anoxic conditions to limit potential toxicity from inactivating the respiratory pathway.  
397 Isolated mutants were passaged on TSA plates containing 0.01% congo red to confirm virulence  
398 plasmid maintenance.

399 *Shigella flexneri* 5a fluorescent strains (wild-type M90T, M90T $\Delta$ *cydAB*, plasmid-cured BS176,  
400 BS176 $\Delta$ *cydAB*, M90T $\Delta$ *fnr* mutant, and BS176 $\Delta$ *fnr* mutant) were generated by transforming the  
401 pFPV25.1 (AmpR) or pDsRed (AmpR) plasmids, as indicated. Antibiotics were added as necessary at  
402 the following concentrations: chloramphenicol, 50  $\mu$ g/mL; ampicillin, 100  $\mu$ g/mL; kanamycin 50  $\mu$ g/mL.  
403 Experiments under different oxygen (O<sub>2</sub>) concentrations were performed in an anaerobic cabinet (Don  
404 Whitley DG250) or in a cabinet in which O<sub>2</sub> tensions can be controlled (Don Whitley H35  
405 Hypoxystation).

406 To assess the level of the T3SS activity, *S. flexneri* 5a was transformed with pTSAR<sup>16</sup>,  
407 allowing the constitutive expression of CFP (cyan) and inducible expression of the fast maturing  
408 eGFP (dependent of the T3SS activity).

### 409 **Cytochrome quantification.**

410 The cellular content of cytochromes *b* and *d* hemes were calculated as described by Dejean et al.<sup>22</sup>,  
411 taking into account the respective molar extinction coefficient values (18.0 km<sup>-1</sup>cm<sup>-1</sup> and 27.9 km<sup>-1</sup>cm<sup>-1</sup>,  
412 respectively) and the reduced minus oxidized spectra recorded using a dual beam spectrophotometer  
413 (Aminco DW2000). Briefly, *S. flexneri* wt,  $\Delta$ *cydAB*, and  $\Delta$ *appCB* mutants strains were grown until

414 OD<sub>600</sub> = 2 was reached. For each measurement, 100 OD units were centrifuged for 10 minutes at  
415 5000 rpm, bacterial pellets were resuspended in distilled water (dH<sub>2</sub>O) up to 2 ml; 1 mL for the  
416 oxidized condition and 1 mL for the reduced condition (dithionite addition). The cytochrome maximum  
417 and minimum absorbance values were measured at 560 and 575, and 630 and 655 nm for  
418 cytochromes *b* and *d*, respectively, and expressed in mol/OD.

## 419 **Cell culture.**

### 420 **Blood collection, Neutrophils purification.**

421 All participants gave written, informed consent in accordance with the Declaration of Helsinki  
422 principles. Peripheral Human blood was collected from healthy patients at the ICAReB service of the  
423 Institut Pasteur (authorization DC No.2008-68). Human blood was collected from the antecubital vein  
424 into tubes containing sodium citrate (3,8% final) as anticoagulant molecules. Guinea pig blood  
425 samples were collected on anesthetized animals by cardiac puncture.

426 Human or guinea pig neutrophils were purified as described previously<sup>23</sup>. Briefly, whole blood  
427 samples were centrifuged at 450x *g* for 15 min. Platelet rich plasma (PRP) was collected and  
428 centrifuged at 2500x *g* for 20 min to form platelet poor plasma (PPP). Blood cells were resuspended in  
429 NaCl 0.9% and dextran sulfate (0.72%). After 30 min sedimentation, the neutrophil-containing upper  
430 layer was centrifuged at 240x *g* for 10 min. The resuspended pellet was separated on a 2-layers  
431 Percoll (GE Healthcare) gradient (51%/42%) by centrifugation at 240x *g* for 20 min. Neutrophils were  
432 collected, and remaining red blood cells were removed using CD235a (glycophorin) microbeads  
433 (negative selection, Miltenyi Biotec).

434 For functional assays, human or guinea pig purified neutrophils were cultured in RPMI 1640  
435 (Life Technologies) supplemented with 10 mM Hepes (Life Technologies).

### 436 **Epithelial cell culture.**

437 The Hep2 cell line was purchased at the ATCC and was tested for mycoplasma contamination. Hep2  
438 epithelial cells were cultured in a DMEM medium (ThermoFischer) supplemented with 10 % Fetal Calf  
439 Serum (ThermoFischer). For functional assays, Hep2 cells were incubated in DMEM medium  
440 supplemented with 10 mM Hepes, without FCS.

### 441 **Antibodies and fluorescent dyes.**

442 Hypoxia detection in guinea pigs was achieved by 2-nitroimidazole derivative EF5 molecule  
443 (University of Pennsylvania, USA) accumulation in tissues. An intracardiac injection (1.5 mL for 150 g  
444 guinea pig) of a 10 mM EF5 solution was performed one hour prior to *Shigella* challenge.

445 EF5 was immunodetected on fixed cells or tissues using an  $\alpha$ -EF5 antibody (ELK3-51)  
446 conjugated with a Cy3 fluorophore (ready-to-use solution, University of Pennsylvania, USA). Dapi  
447 (Invitrogen) was used at 1  $\mu$ g/mL. Neutrophils were labeled with the MUB<sub>40</sub>-Dylight405 marker<sup>12</sup>,  
448 binding to lactoferrin stored in specific and tertiary granules. GLUT-1 was detected with a mouse

449 monoclonal antibody (Abcam, ab40084), used at 1:40 dilution and a secondary antibody conjugated  
450 with an Alexa647 fluorophore (ThermoFisher Scientific).

### 451 **Bacterial cell infection *in vitro*.**

452 Cell entry assays, Hep2 epithelial cells were seeded ( $5 \cdot 10^5$  cells/well) and grown overnight in 24-well  
453 tissue culture plates in indicated conditions (0, 5% and 21% O<sub>2</sub>). Neutrophils were directly seeded  
454 ( $5 \cdot 10^5$  cells/well) in 24-well tissue culture plates. Cells were challenged at an MOI of 100 (Hep2) or 20  
455 (neutrophils) with bacteria grown until the mid-log phase was reached in liquid culture under the same  
456 conditions. Bacteria were spun briefly onto cells by centrifugation at 2000x g for 10 min.

457 To measure bacterial entry, cells were challenged as above, incubated for 30 min at 37°C,  
458 after which gentamicin (50 µg/ml) was added for 30 min to kill extracellular bacteria. Cells were then  
459 washed three times with PBS, lysed with 1 mL 1% saponin in PBS, and bacteria recovered by plating  
460 to solid media. Results are expressed as the number of CFU/ml of cell lysate and are the average of  
461 at least three independent experiments performed in triplicate. Statistical significance was calculated  
462 using the Student's T-test.

### 463 **In vitro O<sub>2</sub> quantification.**

464 Gas proof glass tubes were first left in an anaerobic cabinet to remove all traces of exogenous oxygen  
465 and generate an anoxic atmosphere. The tubes were then filled with RPMI 1640 culture medium  
466 supplemented with 10 mM Hepes pre-stabilized at 37°C and pO<sub>2</sub> = 40 mmHg. Bacteria and  
467 neutrophils were prepared in similar conditions in adequate culture media and resuspended in the  
468 prepared glass tubes. Direct oxygen quantification was performed with a Clark-type sensor mounted  
469 with a needle (Unisense oximeter) over time and initiated immediately after bacteria or cell inoculation.  
470 Results are averaged from at least three independent experiments.

### 471 **Animal models of shigellosis.**

#### 472 **Rabbit ligated ileal loop model.**

473 Experiments on rabbits were approved by the Institut Pasteur local ethic committee (CETEA).

474 For evaluation of competitive indices, experiments were performed on independent occasions  
475 in at least two ileal loops in four animals in total. For competitive indices calculations, bacteria were  
476 grown in liquid media for three hours at 37°C, and a total  $10^7$  CFU of bacteria consisting of equal  
477 numbers of two or three strains in 500 µl of physiological water were injected into loops. After an 18-  
478 hour infection, animals were sacrificed, and bacteria were recovered from the loops. Series of dilutions  
479 of the outputs were plated onto TCS plates containing antibiotics and congo red (CR), allowing the  
480 selection and counting of M90T (CR+ (red colony), Cm<sup>R</sup>, Km<sup>S</sup>), M90TΔ*fnr* (CR+ (red colony), Cm<sup>R</sup>,  
481 Km<sup>R</sup>), BS176 (CR- (white colony), Cm<sup>R</sup>, Km<sup>S</sup>), BS176Δ*fnr* (CR- (white colony), Cm<sup>R</sup>, Km<sup>R</sup>). The  
482 competitive index was calculated as the ratio of mutant to wild-type bacteria recovered from animals  
483 divided by the ratio in the inoculum; the results are the average of at least four samples originating  
484 from four different rabbits. For single strain infections (M90T, BS176, Δ*fnr*, and BS176Δ*fnr*),  $10^7$  CFU



485 were inoculated in ligated loops. After an 18-hour infection, animals were sacrificed and infected ileal  
486 loops collected. For immunohistochemistry, ileal loops were fixed in 4% buffered formalin, embedded  
487 in paraffin, and 5 µm sections obtained and stained with haematoxylin-eosin. *Shigella* strains were  
488 detected using a primary mouse anti-LPS antibody and an HRP-conjugated anti-mouse antibody  
489 (Dako).

#### 490 **Guinea pig intrarectal infection.**

491 Experiments on guinea pigs were approved by the Institut Pasteur local ethic committee (CETEA).

492 Young conventional guinea pigs (3 weeks, female, Dunkin-Hartley, < 150g) were used for  
493 *Shigella* infection and hypoxia detection studies<sup>23</sup>. When indicated, neutropenia was generated in  
494 guinea pigs by two intraperitoneal injections of cyclophosphamide (100 mg/kg on day 7 and 50 mg/kg  
495 on day 1). *Shigella* infection was achieved by an intrarectal challenge of animals with 10<sup>10</sup> CFU  
496 exponentially grown. Infection proceeded for 8 hours before animals were sacrificed and the distal  
497 10 cm of colon harvested and then flushed with 4% paraformaldehyde (PFA) in 1xPBS and inverted  
498 on wooden skewers. Tissues were kept in 4% PFA-1xPBS for 1- to 2-hours to complete fixation and  
499 then incubated in 1xPBS-glycine (100 mM) for 30 minutes to quench the PFA. Tissues were immersed  
500 successively in 15% and 30% sucrose at 4°C overnight and then released from the skewers by a  
501 longitudinal incision and prepared as swissrolls<sup>7</sup>. Swissrolls were embedded in Tissue-Tek OCT  
502 compound (Sakura) using a flash-freeze protocol and frozen at -80°C. For standard  
503 immunofluorescence staining, 10 µm sections were obtained using a cryostat CM-3050 (Leica). For  
504 hypoxia quantitative detection, 30 µm sections were generated.

505 Competitive Indexes were assessed and calculated *in vivo* on homogenized luminal and  
506 colonic mucosa bacteria content (M90T vs M90TΔ*cydAB* mutant and BS176 vs BS176Δ*cydAB*  
507 mutant).

#### 508 **Colonic tissue processing for Quantitative analysis.**

##### 509 **Immunostaining.**

510 For IF samples used for quantitative analyses, transversal colon sections of 30 µm thickness were  
511 stained using a modified protocol from Arena and colleagues<sup>24</sup>. Briefly, tissues on slides were fixed  
512 with 4% PFA for 10 minutes at room temperature. They were then washed with 1xPBS and stained  
513 using an α-EF5-Cy3 antibody solution (supplied by University of Pennsylvania) supplemented with  
514 0.1% Triton, 1% BSA, and MUB<sub>40</sub>-Dylight405 (1 µg/mL) overnight at 4°C. The following day, the slides  
515 were washed with 1xPBS and mounted with ProLongGold® (Invitrogen).

##### 516 **Imaging.**

517 For quantification, fluorescence 3D images were acquired with an automated spinning-disk  
518 microscope (CellVoyager 1000, Yokogawa Electrics, Japan). The swissrolls were first scanned with a  
519 10x air objective (Olympus, UPLSAPO 10x 0.4NA air) in bright-field to locate the tissue, followed by a  
520 scan to locate GFP-expressing *S. flexneri*. Infection foci were imaged with a 40x oil objective  
521 (Olympus, UPLSAPO 40x 1.3NA oil) over 3 fluorescence channels (405, GFP, AF568) and bright field,

522 capturing a 40  $\mu\text{m}$  thick section to encompass the whole tissue. Full fields made of 1x2 to 7x5 3D tiles  
523 of 200  $\mu\text{m}$   $\times$  200  $\mu\text{m}$   $\times$  40  $\mu\text{m}$  each were acquired depending on the size of the given site.

## 524 **Image Quantitative analysis.**

### 525 **Hypoxia profiles through colonic mucosa.**

526 The lamina propria was delineated using Fiji<sup>25</sup>. Intensity profiles were generated from 10  $\mu\text{m}$  thick lines  
527 on maximum-intensity projections of the 3D images in the EF5 channel averaged with a Gaussian filter  
528 with  $\sigma = 10 \mu\text{m}$  (Figure 1a). The profiles ran into the tissue, orthogonally to the lamina propria, and  
529 their location was selected to traverse an infectious focus for infected tissues and randomly arranged  
530 for non-infected tissues.

531 The hypoxia curves of Figure 1b are generated by measuring several profiles that run through  
532 the LP from the apical surface to the basal surface (Figure 1a). Within one condition (infected or non-  
533 infected), all profiles are aligned with respect to the first local maximum (that crosses the LP surface).  
534 After alignment, we have the EF5 signal distribution - one value per profile - as a function of the tissue  
535 depth. We then compute the mean EF5 signal (thick line on Figure 1b) and its standard deviation  
536 (shaded area on Figure 1b) and report them as function of the tissue depth.

537 We then perform a Student t-test at each position along the tissue depth, comparing the  
538 distribution of EF5 signal at a given depth between profiles through tissues of infected (red) and non-  
539 infected (blue) animals, for all depths. We then report the range of depths for which this test reveals  
540 significant differences as black horizontal line over the plot. Figure 1b displays one of three repetitions.  
541 The infected and not-infected curves are made respectively of averaging 128 and 61 profiles. Sample  
542 size was adjusted to reach statistical differences between compared conditions. A blind analysis was  
543 used for image acquisition.

### 544 **Hypoxia measurements at single-cell level.**

545 Automatic segmentation of individual *S. flexneri* and neutrophils was carried out using TrackMate<sup>26</sup>,  
546 yielding their X, Y, and Z coordinates and their local hypoxia levels measured from the EF5 channel  
547 averaged with a 3D Gaussian filter with  $\sigma = 2 \mu\text{m}$ . Together, bacterial and neutrophil positions and the  
548 manual annotations were processed using MATLAB (The MathWorks) for further analysis (Figure 2  
549 and Figure 3).

550 We inspected infection foci manually and estimated their radius to be approximately 16  $\mu\text{m}$ .  
551 Clustered bacteria were therefore defined as bacteria that have at least 6 other bacteria in a  
552 neighborhood of 16  $\mu\text{m}$  in radius from their position (Supplementary Figure 1a). Isolated bacteria were  
553 defined as those having no other bacteria in a neighborhood of a 30  $\mu\text{m}$  radius from their position.  
554 Bacteria that did not fall into these two categories were not included in the analysis (Supplementary  
555 Table 1).

### 556 **Mean hypoxia spatial profile generated by bacteria.**

557 The hypoxia profile around single-bacteria was calculated by averaging the EF5 signal (filtered with  
558  $\sigma = 2 \mu\text{m}$ ) of all pixels at a fixed distance from the closest bacterium (Supplementary Figure 1b). Pixel

559 distance to the closest bacterium was calculated thanks to the image distance transform, taking into  
560 account the non-isotropy of the pixel size (0.2  $\mu\text{m}/\text{pixel}$  in XY and 1  $\mu\text{m}/\text{pixel}$  in Z). Locations outside  
561 of the tissue were not included in the profile. Pixels were then pooled in 1- $\mu\text{m}$  bins from 0 to 50  $\mu\text{m}$ . All  
562 the EF5 intensity of pixels in a single bin contribute to the mean and standard deviation at the bin  
563 distance and build the profiles of Supplementary Figure 2d. Single bins incorporated between 600 and  
564 3.  $10^6$  measurements for a single image. This procedure was repeated on 16 images, treating  
565 separately clustered and dispersed bacteria. These hypoxia profiles average EF5 levels over all pixels  
566 at a specified distance, hereby canceling contributions from other potential sparse hypoxia sources  
567 such as neutrophils.

568 To investigate whether or not neutrophils contribute a significant addition to this hypoxia, we  
569 sought for each neutrophil the closest bacterium and categorized them as dispersed or clustered. We  
570 then reported on the hypoxia profile, the EF5 level, of the neutrophil at the measured distance to the  
571 closest bacterium, respectively, whether the closest bacterium was dispersed or clustered. A one-  
572 sided z-test was used to determine whether or not the neutrophil hypoxia could be explained by the  
573 bacteria hypoxia profile at this distance (dots) or if it was significantly larger (crosses, significance level  
574 at 5%). Less than 5% of neutrophils had a significantly higher hypoxia levels than what was generated  
575 by bacteria over 16 repetitions of this analysis.

#### 576 **Bacteria and neutrophil density.**

577 Whole tissue densities (Supplementary Figure 2a,c-d) were calculated by counting the number of  
578 neutrophils or bacteria, regardless of their clustering status, in the total tissue volume imaged for each  
579 experimental condition.

580 Clustered *Shigella* density (Figure 2d) was calculated by counting the number of neighbors in  
581 a sphere of radius 16  $\mu\text{m}$  around the 61119 clustered bacteria detected in the conventional animals,  
582 the M90T + EF5 condition. Dispersed *Shigella* density was calculated by counting the number of  
583 dispersed bacteria in the volume of the imaged tissue averaged over the 37 tissue sections of the  
584 same condition. Neutrophil density was calculated by counting the number of neutrophils in the  
585 volume of the imaged tissue averaged over a subset of 16 tissue sections of the same condition.

#### 586 **T3SS activity reporter signal analysis.**

587 We expressed the TSAR T3SS activity reporter<sup>2</sup> in *S. flexneri* wild-type strain; EF5 injected guinea  
588 pigs were infected with this strain as described above. The reporter emits in the Cyan channel (CFP)  
589 for all bacteria and in the Green channel for bacteria that are positive for TS3 activity (fast-maturing  
590 eGFP, Rep+). GFP level corresponding to an active T3SS (Rep+) was determined *in vitro* by culturing  
591 *S. flexneri* 5a pTSAR in the presence or absence of oxygen, with or without congo red (0.01%). More  
592 than 100 individual bacteria were analyzed in each condition *in vitro*. We then imaged tissue sections,  
593 focusing on bacteria foci and proceeded to a similar analysis. We quantified signals in 2488 WT  
594 bacteria located in foci of infection.

## 595 **Statistical analysis.**

596 All statistical analyses have been performed with MATLAB software (The MathWorks). Comparisons  
597 with two groups (Figures 1b, 1h, 1i, 2b) were supported with Student unpaired-*t* tests. Comparisons  
598 with three groups or more were supported by 1-way ANOVA test (Figures 1f, 3d, 3e, 4b and  
599 Supplementary Figures 4b,d-e) and 2-way ANOVA test (Figures 2g, 3b and Supplementary Figure  
600 4c), followed by a *post hoc* Tukey test.

601 When *p*-values for the significance of pairwise comparisons were calculated (either from a  
602 Student-*t* test or a *post hoc* Tukey test after an ANOVA test) and displayed on figures, we used the  
603 following convention:

- 604 • *ns* not significant;  $p \geq 0.05$ ;
- 605 • \*  $p < 0.05$  &  $p \geq 0.01$ ;
- 606 • \*\*  $p < 0.01$  &  $p \geq 0.001$ ;
- 607 • \*\*\*  $p < 0.001$ .

## 608 **Box-plots.**

609 When results are presented in the shape of a box-plot (Figures 1f, 1h, 1i, 2b), the central mark  
610 indicates the median, and the bottom and top edges of the box indicate the 25<sup>th</sup> and 75<sup>th</sup> percentiles,  
611 respectively. The whiskers extend to the most extreme data points not considered outliers, and the  
612 outliers are not plotted. Outliers are data points that are further away than 1.5 times the range from the  
613 1<sup>st</sup> to the 3<sup>rd</sup> quartile, respectively above or below the 3<sup>rd</sup> and 1<sup>st</sup> quartile.

## 614 **Direct oxygen consumption quantification *in vitro*.**

615 Direct oxygen quantifications were performed in gas-proof glass punchable tubes (BD Vacutainer Z,  
616 reference 368430) using an oximeter (OXY-Meter, Unisense) combined with a needle sensor for  
617 piercing (OX-NP). Data was recorded using the SensorTrace logger software (Unisense). Glass tubes  
618 were first opened in an anaerobic cabinet (MiniMac DG250, Don Withley) for 30 min to ensure that all  
619 traces of exogenous oxygen were removed from the tube (anoxic atmosphere). Such conditioned  
620 tubes were subsequently filled with 2 mL of a culture medium (RPMI 1640 + 10 mM Hepes for  
621 neutrophils), pre-stabilized at 37°C and at  $pO_2 = 40$  mmHg (5%  $O_2$ ) in a hypoxic chamber (In vivo 500,  
622 Don withley) (Figure 2e). Prior to their inoculation, bacteria (*S. flexneri* 5a wild-type and mutant strains,  
623 *E. coli*, *S. typhimurium*, *L. monocytogenes*, *S. aureus* or *L. casei*) were grown in similar conditions until  
624  $OD_{600} = 0.3$  was reached. Bacteria alone or with neutrophils were resuspended at the indicated  
625 concentrations in RPMI 1640 + 10 mM Hepes. When indicated Diphenyliodonium chloride (DPI,  
626 Sigma-Aldrich) was added at a 25  $\mu$ M final concentration, N-Formyl-Met-Leu-Phe (FmlF, Sigma-  
627 Aldrich) at 1  $\mu$ M. Direct oxygen quantification were performed over time and initiated immediately after  
628 bacteria or cell inoculation. Results were averaged from at least three independent measurements.

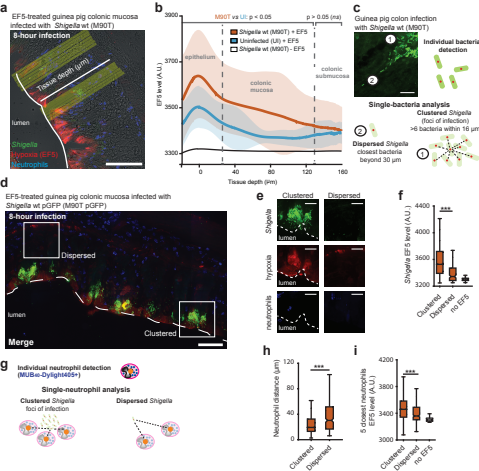
629 **Data availability.**

630 The datasets generated and/or analyzed during the current study are available from the corresponding  
631 author on reasonable request.

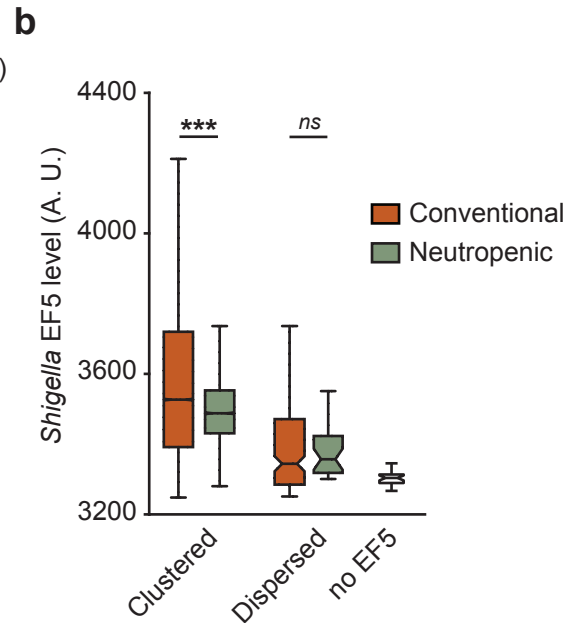
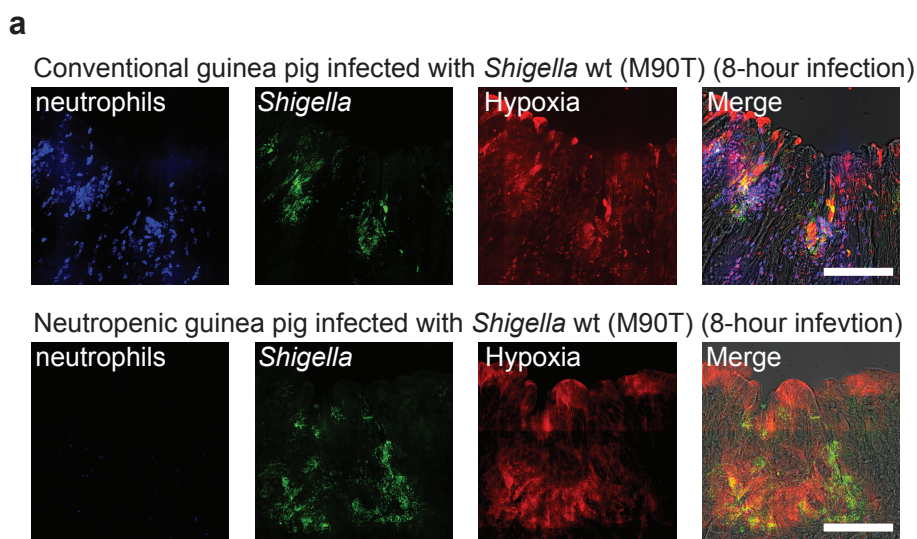
632 **References**

- 633 1. Marteyn, B. *et al.* Modulation of Shigella virulence in response to available oxygen in  
634 *in vivo*. *Nature* **465**, 355–358 (2010).
- 635 2. Cramer, T. *et al.* HIF-1alpha is essential for myeloid cell-mediated inflammation. *Cell*  
636 **112**, 645–657 (2003).
- 637 3. Peyssonnaud, C. *et al.* HIF-1alpha expression regulates the bactericidal capacity of  
638 phagocytes. *J. Clin. Invest.* **115**, 1806–1815 (2005).
- 639 4. Walmsley, S. R. *et al.* Hypoxia-induced neutrophil survival is mediated by HIF-1alpha-  
640 dependent NF-kappaB activity. *J. Exp. Med.* **201**, 105–115 (2005).
- 641 5. Huether, S. E. & McCance, K. L. *Understanding Pathophysiology*. (Elsevier Health  
642 Sciences, 2015).
- 643 6. Karhausen, J. *et al.* Epithelial hypoxia-inducible factor-1 is protective in murine  
644 experimental colitis. *J. Clin. Invest.* **114**, 1098–1106 (2004).
- 645 7. Campbell, E. L. *et al.* Transmigrating Neutrophils Shape the Mucosal  
646 Microenvironment through Localized Oxygen Depletion to Influence Resolution of  
647 Inflammation. *Immunity* (2014). doi:10.1016/j.immuni.2013.11.020
- 648 8. Arena, E. T., Tinevez, J.-Y., Nigro, G., Sansonetti, P. J. & Marteyn, B. S. The  
649 infectious hypoxia: Occurrence and causes during Shigella infection. *Microbes Infect.*  
650 2017 Mar;19(3):157-165
- 651 9. Ziemer, L. S. *et al.* Noninvasive imaging of tumor hypoxia in rats using the 2-  
652 nitroimidazole 18F-EF5. *Eur. J. Nucl. Med. Mol. Imaging* **30**, 259–266 (2003).
- 653 10. Bumann, D. Heterogeneous host-pathogen encounters: act locally, think globally. *Cell*  
654 *Host Microbe* **17**, 13–19 (2015).
- 655 11. Davis, K. M. & Isberg, R. R. Defining heterogeneity within bacterial populations via  
656 single cell approaches. *Bioessays* **38**, 782–790 (2016).
- 657 12. Anderson, M. C. *et al.* MUB<sub>40</sub> Binds to Lactoferrin and Stands as a Specific Neutrophil  
658 Marker. *Cell Chem Biol* Apr 19;25(4):483-493 (2018)
- 659 13. Sheridan, W. G., Lowndes, R. H. & Young, H. L. Intraoperative tissue oximetry in the  
660 human gastrointestinal tract. *Am. J. Surg.* **159**, 314–319 (1990).
- 661 14. Uden, G. & Trageser, M. Oxygen regulated gene expression in Escherichia coli:  
662 control of anaerobic respiration by the FNR protein. *Antonie Van Leeuwenhoek* **59**,  
663 65–76 (1991).
- 664 15. Way, S. S., Sallustio, S., Magliozzo, R. S. & Goldberg, M. B. Impact of either elevated  
665 or decreased levels of cytochrome bd expression on Shigella flexneri virulence. *J.*  
666 *Bacteriol.* **181**, 1229–1237 (1999).
- 667 16. Campbell-Valois, F.-X. *et al.* A fluorescent reporter reveals on/off regulation of the  
668 Shigella type III secretion apparatus during entry and cell-to-cell spread. *Cell Host*  
669 *Microbe* **15**, 177–189 (2014).
- 670 17. Davis, K. M., Mohammadi, S. & Isberg, R. R. Community behavior and spatial  
671 regulation within a bacterial microcolony in deep tissue sites serves to protect against  
672 host attack. *Cell Host Microbe* **17**, 21–31 (2015).
- 673 18. Hughes, E. R. *et al.* Microbial Respiration and Formate Oxidation as Metabolic  
674 Signatures of Inflammation-Associated Dysbiosis. *Cell Host Microbe* **21**, 208–219  
675 (2017).
- 676 19. Nizet, V. & Johnson, R. S. Interdependence of hypoxic and innate immune responses.

- 677 *Nat. Rev. Immunol.* **9**, 609–617 (2009).
- 678 20. Taylor, C. T. & Colgan, S. P. Regulation of immunity and inflammation by hypoxia in  
679 immunological niches. *Nat. Rev. Immunol.* **17**, 774–785 (2017).
- 680 21. Light, S. H. *et al.* A flavin-based extracellular electron transfer mechanism in diverse  
681 Gram-positive bacteria. *Nature* **562**, 140–144 (2018)
- 682 22. Dejean, L., Beauvoit, B., Guérin, B. & Rigoulet, M. Growth of the yeast  
683 *Saccharomyces cerevisiae* on a non-fermentable substrate: control of energetic yield  
684 by the amount of mitochondria. *Biochim. Biophys. Acta* **1457**, 45–56 (2000).
- 685 23. Monceaux, V. *et al.* Anoxia and glucose supplementation preserve neutrophil viability  
686 and function. *Blood* **128**, 993–1002 (2016).
- 687 24. Arena, E. T. *et al.* Bioimage analysis of *Shigella* infection reveals targeting of colonic  
688 crypts. *Proc. Natl. Acad. Sci. U.S.A.* **112**, E3282–90 (2015).
- 689 25. Schindelin, J. *et al.* Fiji: an open-source platform for biological-image analysis. *Nat.*  
690 *Methods* **9**, 676–682 (2012).
- 691 26. Tinevez, J.Y. *et al.* TrackMate: an open and extensible platform for single-particle  
692 tracking. *Methods* **115**, 80–90 (2017).
- 693
- 694
- 695

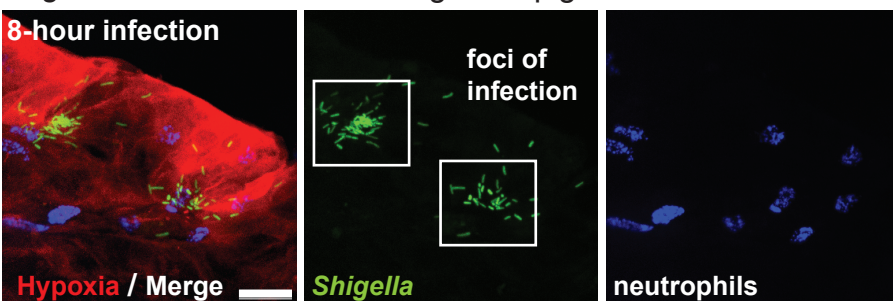






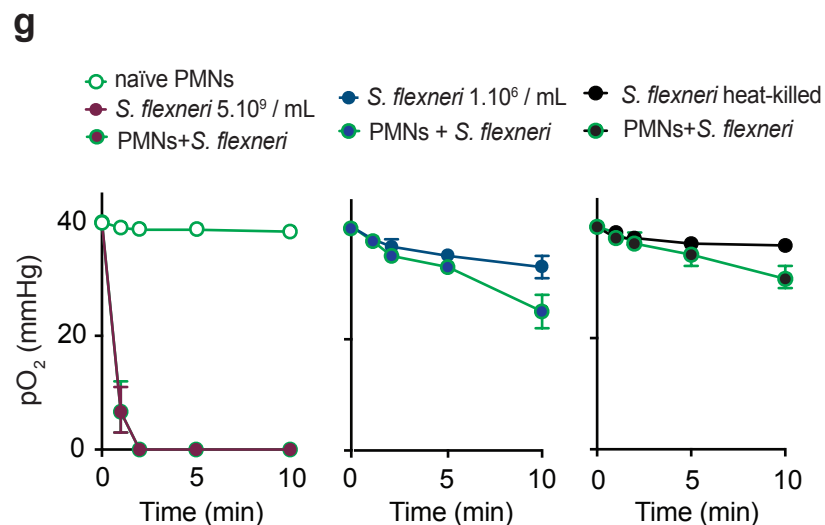
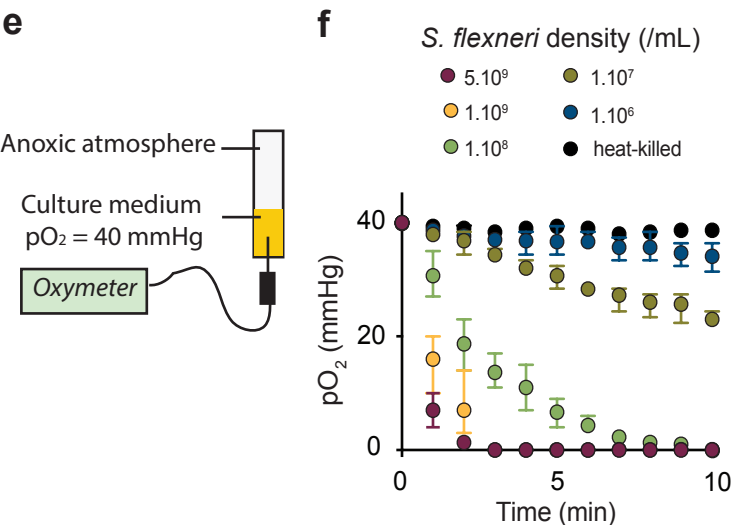
**c**

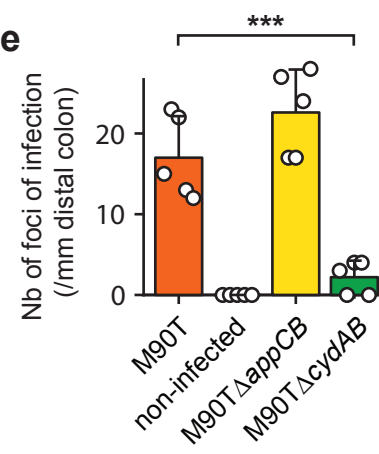
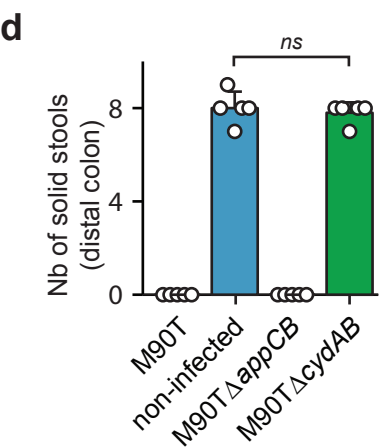
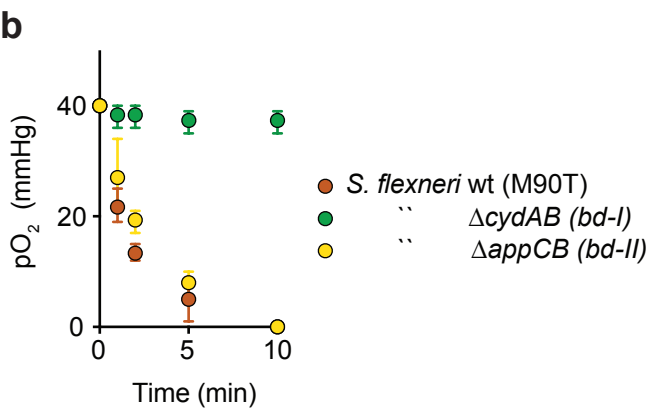
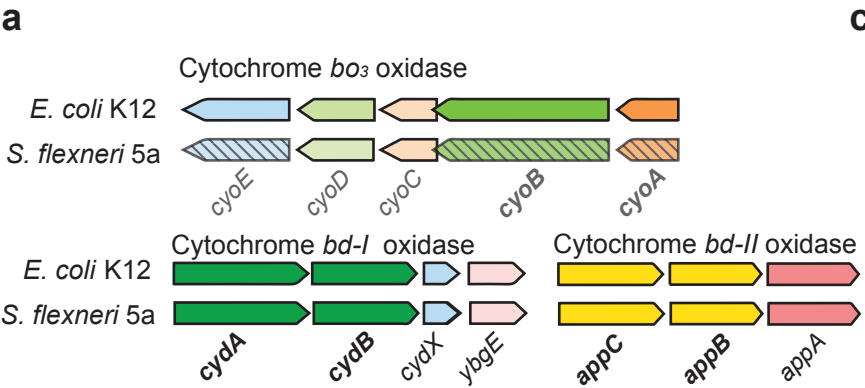
*Shigella* foci of infection in the guinea pig colonic mucosa



**d**

	cell density (/mL) mean +/- s.d.	n
clustered <i>Shigella</i>	$3.9 \cdot 10^9 \pm 2.7 \cdot 10^9$	61119
dispersed <i>Shigella</i>	$1.3 \cdot 10^6 \pm 1.1 \cdot 10^6$	37
neutrophils	$8.1 \cdot 10^7 \pm 5.4 \cdot 10^7$	16





**f** Guinea pig colon co-infected with *S. flexneri* wild-type and/or *DcydAB* mutant strains (8-hour infection)

